Journal of
Ship&Ocean
Technology
JUNE 2004

SOTECH Vol. 8, No. 2, pp. 29~40, 2004

A Parametric Study on Ice Scouring Mechanism for Determination of Pipeline Burial Depths

Kyung-Sik Choi[1] and Jong-Ho Lee[1]

[1] Division of Ocean Development Engineering, Korea Maritime University, Busan, KOREA;
E-mail: kchoi@hhu.ac.kr

Abstract

Interaction of grounded ice ridges with underlying seabed is one of the major considerations in the design of Arctic pipeline system. Previously several ice scour models were developed by researchers to describe the ice scour-seabed interaction mechanism. In this paper, a parametric study on ice scouring mechanism is performed and the limitation of ice scour-seabed interaction models is discussed. Simple laboratory tests are carried out and then the shape pattern of deposited soil around the ice is redefined. New ice scour model assumes trapezoidal cross section based on the field observation data. Ice scour depth and soil resistance forces on seabed are calculated with varying the keel angle of a model ice ridge.

Keywords: Arctic Offshore Pipelines, Ice Scour-Seabed Interaction Models, Trapezoidal Cross Section, Scour Depth, Soil Resistance Force

1 Introduction

Seabed scour by ice keels is often found in Arctic seas, especially in the shallow coastal regions (Figure 1). The interaction of grounded ice ridge with the underlying seabed is an important design factor for Arctic pipeline systems. During the ice scour process the force exerted by the ice features on the seabed is much greater than the strength of the pipelines, hence it causes severe damage to pipelines. Pipelines not only need to be buried below the maximum scour depth, but also deep enough below the scour to avoid excessive bending strains caused by soil deformations (Figure 2).

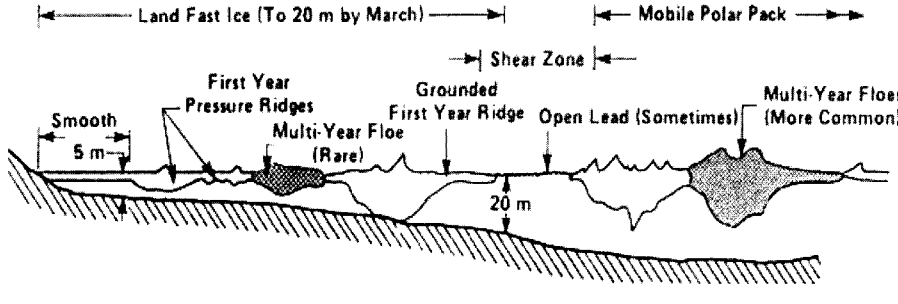

Figure 1: Typical cross sections of sea ice formation in the Arctic (from Croasdale 1977)

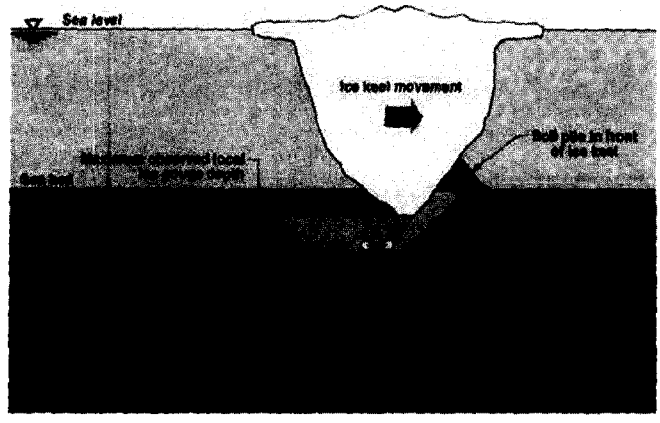

Figure 2: Ice keel movement (from Nogueira and Paulin 1999)

In order to estimate appropriate burial depths for Arctic offshore pipelines, ice scour mechanism must be fully understood. Studies have been carried out to investigate ice scour geometry from field observation data. Field observations require significant time and often neglect the ice scour mechanism itself. Experimental techniques were also used for ice scour study. From model test results, the correlations among major parameters that influence the ice scour-seabed interaction process, and ice forces exerted on the underlying seabed, can be estimated.

Theoretical and numerical methods are best used in parallel with experimental methods. Previously several ice scour models were developed by researchers to describe the ice scour-seabed interaction mechanism. In this paper, a parametric study on ice scouring mechanism is performed and the limitation of ice scour-seabed interaction models is discussed. Simple laboratory tests are carried out and then the shape pattern of deposited soil around the ice model is redefined and a new ice scour model is proposed. The new model assumes trapezoidal cross sections representing typical shape of an ice ridge based on the field observation data. Ice scour depth and soil reacting forces on seabed are calculated with varying the keel angle of an ice ridge.

2 Various Ice Scour Models

So far several ice scour models have been introduced. First, Chari (1979) studied an ice scour mechanism during horizontal motion of a rectangular ice block. He suggested a simple ice scour model assuming that the ice scour process stops when the entire kinetic energy of ice dissipates through the plastic deformation and friction of the soil. In his model, vertical motion or rotation of the ice model was not considered. Later Kioka and Saeki (1995) performed a series of tests with a rectangular ice model of constant speed and they developed a scour model to estimate the driving forces on the ice model. Yoon et al. (1997) studied ice scouring by combining Chari's and Kioka's models to express decelerating horizontal and vertical motions. Yang (1999) assumed a trapezoidal cross section of the ice ridge and applied Coulomb's passive pressure expression to calculate soil resistance forces. Yoon et al. and Yang used simple linear gouging curves instead of the parabolic curves used in Kioka's model. Recently Kioka et al. (2000) developed an ice model with trapezoidal cross sections and skills of model test on ice scour events.

Figure 3 shows the idealized soil patterns around the ice models previously used by

researchers, Chari (1979), Kioka and Saeki (1995), Yoon et al. (1997) and Yang (1999) respectively. The length of the disposed soil on front face and soil resistance force in horizontal direction are calculated for each ice scour model. In Figure 4, rectangular section ice models were assumed. As the scouring event proceeds, the amount of disposed soil on side face of ice model increases much faster than the disposed soil on front face and the soil resistance force in horizontal direction also increases. Yoon's model gives the largest soil resistance force among three scour models because it includes both the disposed soil on front face and soil on side face of the ice model.

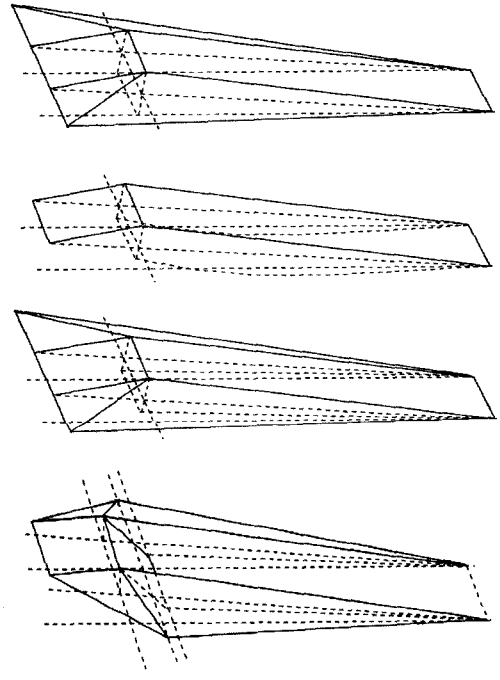

Figure 3: Idealization of disposed soil patterns in the ice scour models (Chari 1979; Kioka and Saeki 1995; Yoon et al. 1997; Yang 1999)

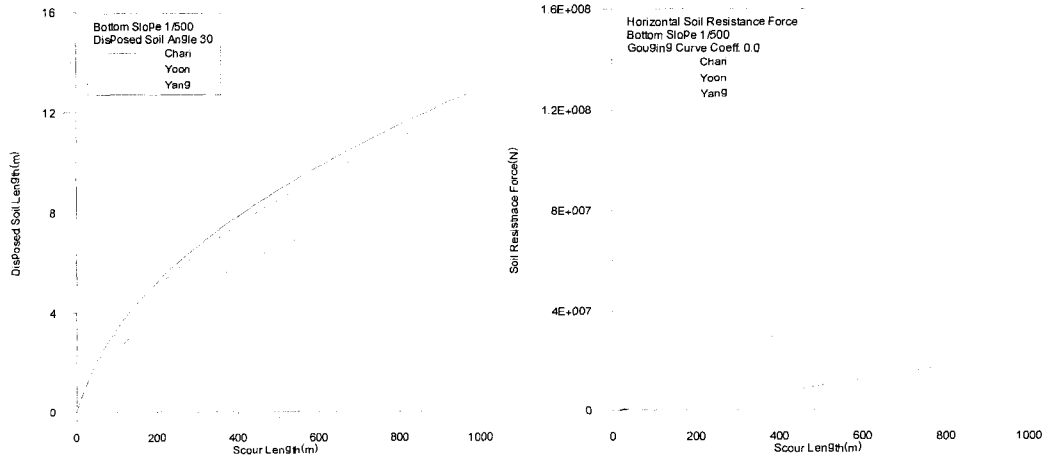

Figure 4: Disposed soil length on the front face and soil resistance force in horizontal direction

3 Ice Scour Experiments

Since the shape pattern of deposited soil around the ice model is important in ice scour modeling, in this study a series of simple laboratory tests were carried out. The test basin (4 m x 0.8 m x 0.6 m) was set up and ice models filled with sand for simulating proper draft and density were made of plywood panel. Ice models were towed under constant pulling forces and then the shape pattern of deposited soil and scour depth, scour length were measured. As seen in Figure 5, the test models have trapezoidal cross sections representing typical shape of an ice ridge and the keel angle of the model varies 0°, 30°, 45°, 60°. Seabed slope was selected as 1/10, 1/20, 1/30 and 1/40 respectively. For variation of internal friction angle of soil, several types of sand with different grain sizes were used.

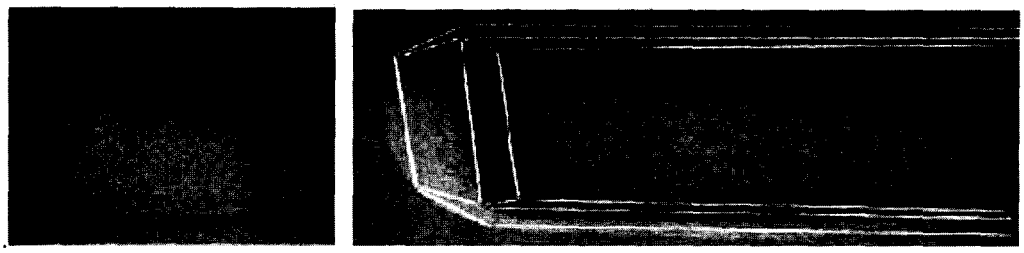

Figure 5: Photos of laboratory model test and an idealized soil pattern

Table 1: Slopes of disposed soil on the front and side faces (seabed slope 1/30)

Ice Keel Angle	Disposed Soil Length (front)	Disposed Soil Height (front)	Disposed Soil Length (side)	Disposed Soil Height (side)	Disposed Soil Angle (front)	Disposed Soil Angle (side)
0°	11 cm	5.8 cm	4 cm	2.8 cm	27.8°	34.9°
30°	10.5 cm	4.5 cm	2.5 cm	1.7 cm	23.2°	34.2°
45°	9.5 cm	4.3 cm	2 cm	1.5 cm	24.4°	36.9°
60°	6.3 cm	3.5 cm	2.5 cm	1.8 cm	29.1°	35.8°

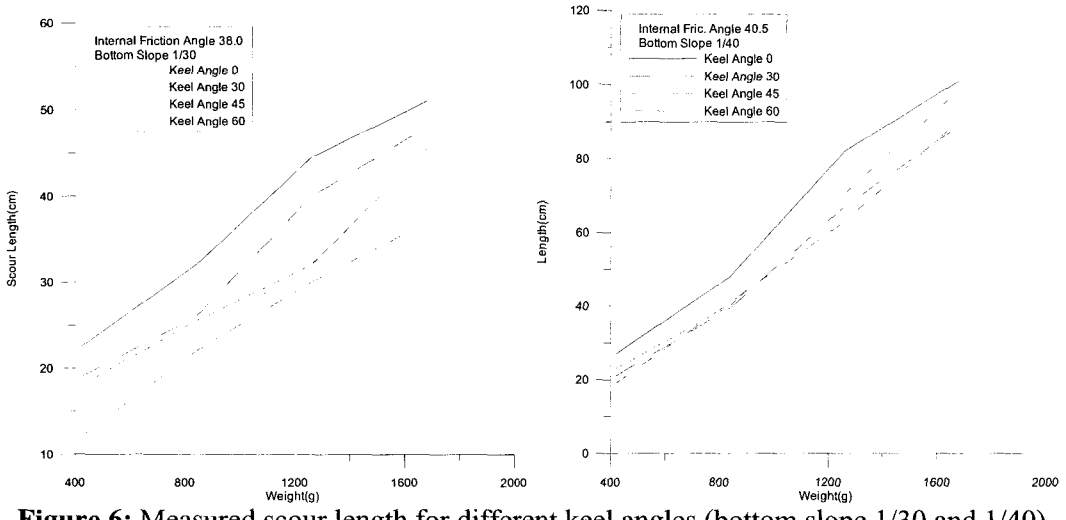

Figure 6: Measured scour length for different keel angles (bottom slope 1/30 and 1/40)

It can be seen from Table 1 that for smaller ice keel angles the disposed soil length and height gets larger. However, the angles of disposed soil are almost same regardless of keel angles or seabed bottom slopes. Figure 6 shows the effect of varying keel angles on scouring characteristics. With the increase of keel angles the scour length of seabed soil increases. With increase of internal friction angle, the scour length of seabed soil also increases. For smaller grain size, the internal friction angle is large and the friction between soil and the wall increases.

4 Modification of scour models

Shapes of the Ice Model and Soil Equation

Ice drifts with a certain velocity imposed by wind and current, and moves over the seabed according to soil resistance forces in vertical and horizontal directions. In the development of the ice scour model it is assumed that the seabed soil is strong enough to support ice motion in the vertical direction and soil scoured by the ice is completely disposed of to the front and to the sides of the ice. In this process, assuming plastic deformation of soil, volume change of soil is not considered. In Figure 7, from the field observation, an ice ridge is idealized as one with a trapezoidal cross section for representing ice features often found in shallow Arctic seas (Wright et al. 1981). The approximate ratio of sail height to keel depth and sail angle are selected from published statistical data. The total cross-sectional area of the ice ridge is given by

$$A = H^2 \cot 20^\circ + 0.5 \times (B_b + l_i) \times h_i \tag{1}$$

where H : sail height of ice ridge
h_i : keel depth of ice ridge
B_b : breadth of keel bottom
l_i : breadth of ice ridge at waterline

During the interaction process various types of soil resistances and forces act on the ice model and they increase as the scouring proceeds. The resistances and forces include frontal and side soil pressure, vertical reaction and friction forces and weight and buoyancy of ice. Assuming no volume changes, the total volume of scoured soil is the volume in horizontal motion minus the displaced volume during vertical motion as in Eq.(2). It equals the volume of surcharged soil in front and to the sides of the ice model. After first contact between the ice and seabed, ice transverses into the soil. Due to the inclined surface of the seabed, horizontal movement causes vertical elevation and scour depth changes. Because the reaction force between ice and seabed has a vertical component, ice moves to equilibrium position of effective weight of ice and soil reaction force. Since the seabed slope is very small, a linear function is used for the gouging curve to calculate vertical elevation of the ice model. Soil equation Eq.(2) reduces to a cubic equation in terms of the front surcharged soil length L_1 in horizontal direction.

$$\frac{1}{2}BL^2 \tan\beta - B\int_0^L \zeta(x)dx + \frac{1}{2}Bd^2C_1 = \frac{1}{2}BL_1^2k_1(1+k_1C_1) + \frac{1}{3}(L_1 + L_1k_1C_1 + dC_1 + L)(L_1k_1)^2 \cot\alpha \tag{2}$$

where α : angle of the front surcharged soil slope
β : angle of seabed slope
ω : ice keel angle
L : total scour length
$\zeta(x)$: ice gouging curve defined as a linear function of x

$$\tan\alpha + \tan\beta = k_1$$

$$C_1 = \frac{\tan\omega}{1 - \tan\omega\tan\beta}$$

$$d = L\tan\beta - \zeta(L)$$

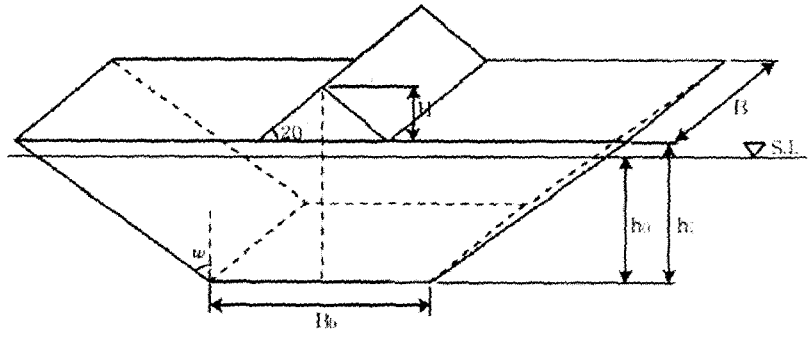

Figure 7: Idealized ice ridge model with a trapezoidal cross section

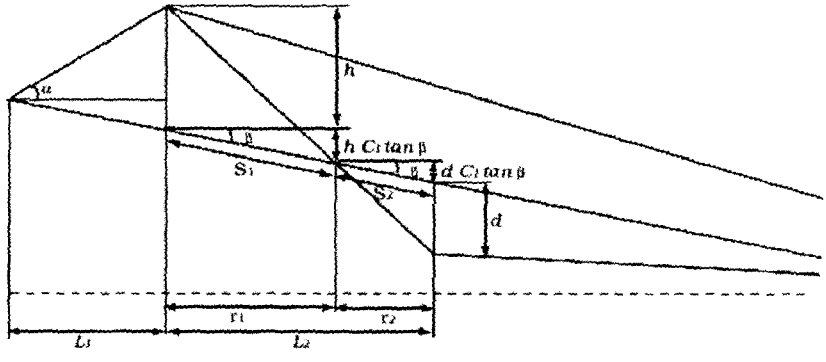

Figure 8: Side profile of disposed soil around an ice ridge model

Energy Balance Equation

Ice scour depth and the interaction force are calculated by solving the energy balance equation, Eq.(3). Initial kinetic energy of the ice ridge is completely dissipated through work done by soil resistance forces and drag forces. Soil resistance forces consist of passive earth pressure and frictional forces between ice and soil.

$$E_k = \int_0^L P_{sx}\,dx + \int_0^{\zeta(L)} P_{sy}\,dy - \int_0^L F_d\,dx + E_p \qquad (3)$$

where E_k : kinetic energy of the ice ridge
P_{sx} : soil resistance force in the x-direction

P_{sy} : soil resistance force in the y-direction
F_d : drag force by wind and current
E_p : potential energy of the ice ridge

Earth Pressure
Coulomb's passive earth pressure theory is applied to the calculation of soil resistance force. Both wall friction angles acting on front face and on side faces of ice are considered. Passive earth pressure acting on the front face of the ice feature is;

$$P_f = \frac{1}{2} K_{pf} \rho_s g h_f^{\,2} B \tag{4}$$

where $h_f = (h + d)(1 + C_1 \tan \beta)$
K_{pf} : coefficient of passive earth pressure on front face of ice model
ρ_s : submerged density of saturated soil
g : gravitational acceleration
ϕ : internal friction angle of soil
φ : angle of surcharged soil with respect to seabed slope

The passive earth pressure acting on the side face of ice model is;

$$P_s = \int_0^{d \cot \beta} \int_0^{\varepsilon \tan \beta} \rho_s g K_{ps} \eta \; d\eta d\varepsilon \tag{5}$$

where η : dummy variable for integration along gouging curve
ε : elevation of gouging curve
K_{ps} : coefficient of passive earth pressure on side face of ice model

Friction Forces
Friction force in the x-direction, K_x consists of friction on front face, P_{ftx}, friction on side faces, P_{sf} and friction on bottom of ice, μK_y;

$$K_x = P_{ftx} + P_{sf} + \mu K_y \tag{6}$$
$$K_y = P_{fty} + P_{sf} + W_e - (m + m_a) a_y \tag{7}$$

where K_y : contact force or reaction force in y-direction at the bottom
W_e : effective weight of ice ridge
m_a : added mass of ice ridge
a_y : acceleration of ice ridge in the y-direction

5 Sample Calculation

Input parameters for the sample calculation to analyze ice-seabed interaction are properties of ice, soil and other environmental factors such as the shape and size of ice, types of seabed soil

and internal friction angle, unit weight of soil, seabed slope, slope of surcharged soil etc. Data for sample calculation is shown in Table 2 and results are given in Figures 9~13.

Table 2: Data for sample calculation

Properties	Symbols	Initial Value
Ice	H	7.9 m
	B_b	variable
	ω	0 - 60°
	B	35 m
	ρ_i	917 kg/m^3
Soil	ρ_s	1,500 kg/m^3
	ϕ	30 °
	α	33.02°
Environments	β	1/500 , 1/1000
	v_0	1.3 m/s
	ρ_w	1,024 kg/m^3
	ρ_a	1.0 – 3.0 kg/m^3
	C_d	0.1, 0.2, 0.3
	C_m	0.5
	μ	0.1

For each model of different keel angle, Figure 9 shows calculated scour depths while varying kinetic energy of ice ridge, i.e., varying ice mass. As initial kinetic energy of the ice ridge increases, scour depth increases, but less rapidly. From the figures it is found that the proposed ice scour model is sensitive to wall friction angle and that the smallest scour depth is obtained for the model with the sum of keel angle and wall friction angle to be about 60°.

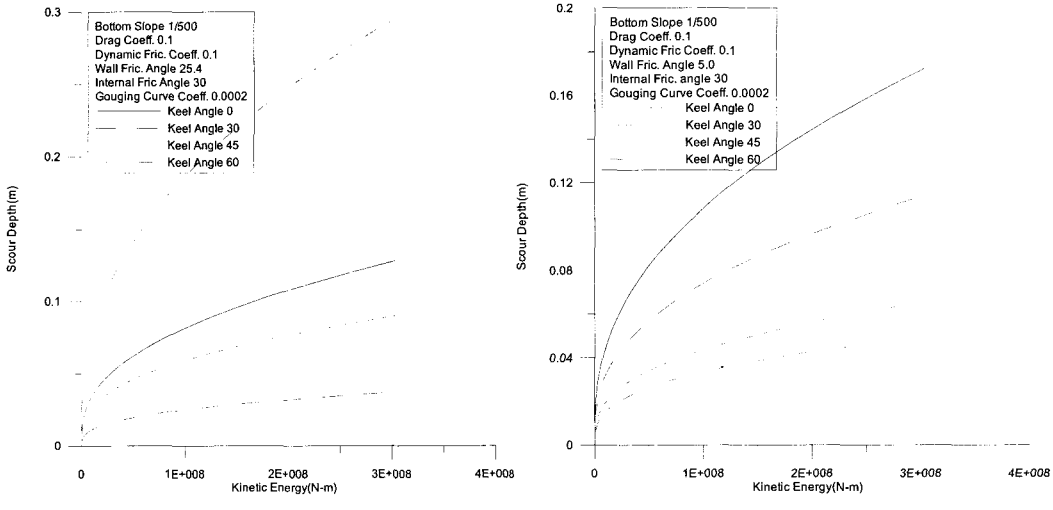

Figure 9: Scour depth changes with keel angle variation (wall friction angle 25.4° and 5.0°)

For different keel angles Figure 10 shows calculated soil resistance forces in the horizontal direction while varying kinetic energy of the ice ridge. The largest resistance force is

calculated for the model with the sum of keel angle and wall friction angle to be about 60°, which is the direction of soil resistance force, i.e., the angle of the resistance force with respect to the horizontal plane. The larger the soil resistance force is, the smaller the scour depth is.

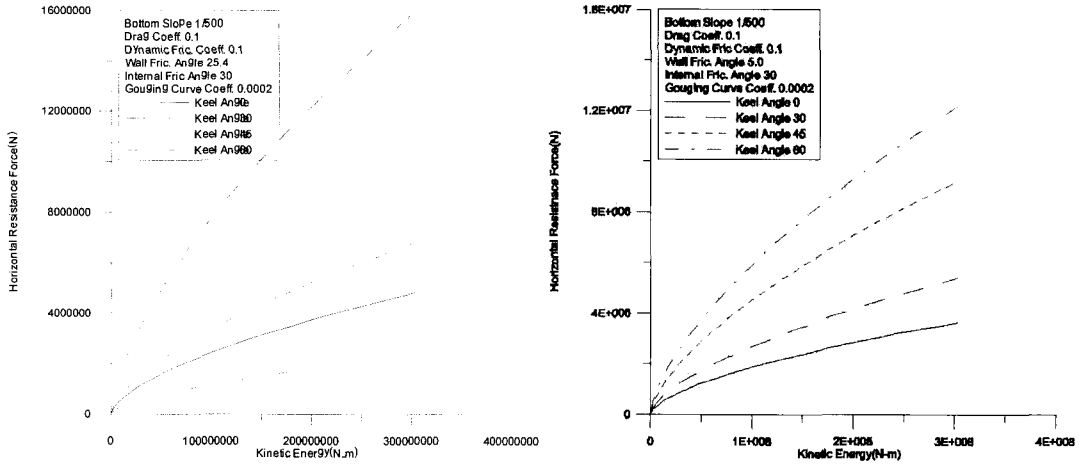

Figure 10: Horizontal soil resistance with keel angle variation (wall friction angle 25.4° , 5.0°)

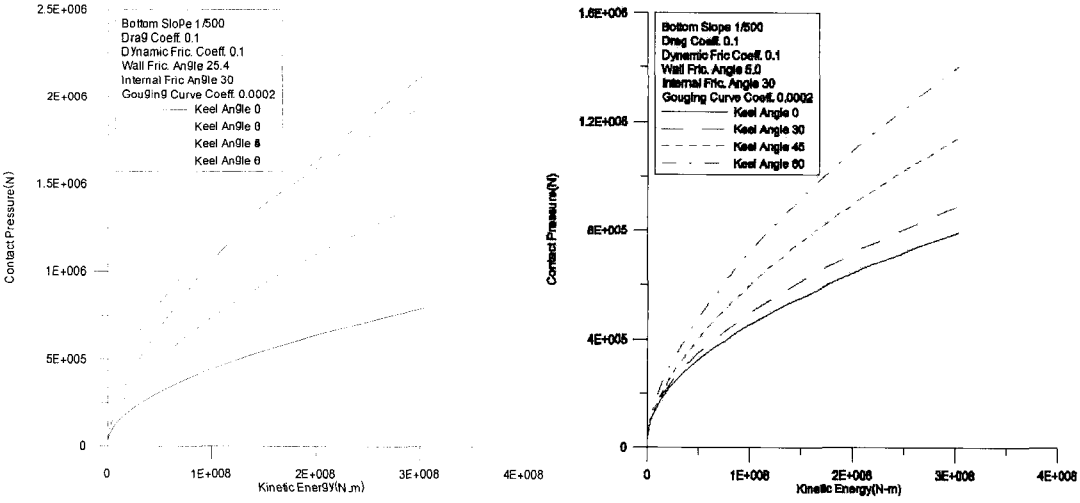

Figure 11: Contact pressure changes with keel angle variation (wall friction angle 25.4° , 5.0°)

In vertical direction, Figure 11 shows that the contact pressure at the bottom of ice ridge again reaches its maximum for the model with the sum of keel angle and wall friction angle to be about 60°. Slight elevation can cause a great effect on vertical reaction force. Figure 12 shows the transmitted stresses through soil foundation and it is found that the stress distribution is more localized for the model with a keel angle of 60° than the other models. For the model with a keel angle of 60° the stresses decrease rapidly up to the depth of 20 m and then slowly decrease below 20 m. However the stress level is somewhat high even at the

depth of 60 m. Because of the trapezoidal geometry, the contact area gets smaller and the transmitted stress larger, as the keel angle increases.

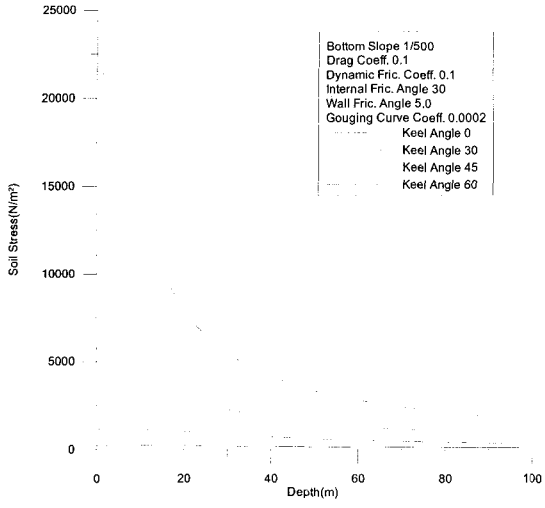

Figure 12: Stresses transmitted through seabed soil

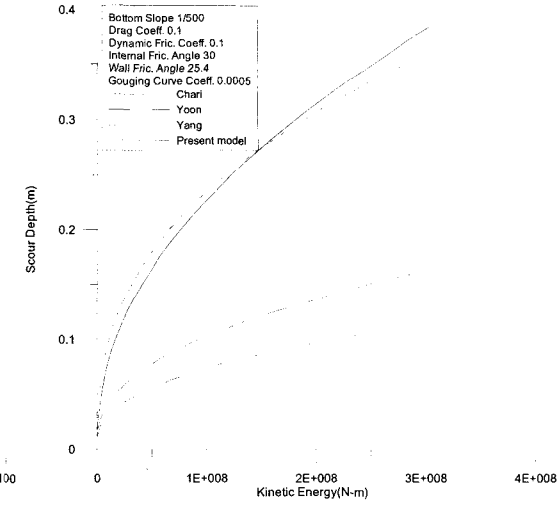

Figure 13: Comparison of scour models

In Figure 13, proposed model is compared to previously developed ice scour models. With the keel angle to be 0°, i.e., a rectangular cross section, the proposed model estimates smaller scour depth than Chari (1979) or Yoon et al. (1997) does. This means that the proposed ice scour model is the one that calculates larger soil resistance force. The reason why previous two models give larger scour depths than our model may be explained by comparing the patterns of surcharged soil, especially the corner wedge, around the ice models as seen in Figure 3.

Table 3: Comparison of the proposed model calculation with field data

	Ice Size (m)	Seabed Bottom Slope	Observation (ice speed, scour depth)	Scour Depth: Present Model	Scour Depth : Yoon et al. (1997)
Sakhalin Offshore	200×20×30 (L×B×H)	1/100	V_0 = 1.5 m/s d = 0.5-1.0 m dmax =2.13 m	0.78 m	1.0 m
		1/1000		0.21 m	0.29 m
Canadian Beaufort Sea	2000×20×30 (L×B×H)	1/100	V_0 = 0.5 m/s d = 0.6-2.1m dmax = 4.6 m	0.45 m	0.68 m
		1/1000		0.15 m	0.21 m
Environ-mental Conditions	Drag coefficient = 1.0 Internal friction angle = 0°, 30° Water density = 1,024 kg/m^3 Soil density = 1,500 kg/m^3 Gouging curve coefficient = 0.0002 Keel angle = 60° Wall friction angle = 25.4°				

Table 3 is a comparison of the proposed model calculation with field observation data for Sakhalin offshore (Gulati 1994) and Canadian Beaufort Sea (Palmer 1989). As shown in Table 3, sample calculation results are not far from usual observation data 0.5-1.0 m for Sakhalin offshore. Calculation is a little out of bound for Beaufort Sea, 0.6-2.1 m. Regarding the variation and uncertainty in environmental factors, especially in soil properties, the calculated results fall within the acceptable range of observed values. However a further effort for the model verification is required to compare the proposed model with available field data.

Conclusions

Regarding accurate estimation of pipeline burial depths, the proposed ice ridge model adopts a more realistic trapezoidal cross section. Shape pattern of the surcharged soil is newly defined based on field observation and model experiments. With this model, the ice scour depth and soil resistance forces during the scouring process are calculated varying keel angles of an ice model. The calculation is performed for the various ice conditions through a parametric study to find the effect of various environmental parameters on ice scour depth. For different keel angles, as initial kinetic energy of ice ridge increases, scour depth increases. Calculated results of the proposed ice scour model are compared to field observation data for Sakhalin offshore and Canadian Beaufort Sea. The calculated results fall within the acceptable range of observed values.

Acknowledgements

This work is a part of a project supported by the Korean Science and Engineering Foundation through ASERC (Contract R11-2002-008-01002-0).

References

Chari, T.R. 1979. Some geotechnical aspects of iceberg scours on ocean floors. Canadian Geotechnical Journal, 16, 379-390.

Croasdale, K.R. 1977. Ice engineering for offshore petroleum exploration in Canada. Proc. 4th International Conference on Port and Ocean Engineering under Arctic Conditions, St. John's, Canada, 1-32.

Gulati, K.C. 1993. Design concepts for sakhalin offshore production platforms. Proc. 12th International Conference on Port and Ocean Engineering under Arctic Conditions, Hamburg, Germany, **2**, 487-496.

Kioka, S. and H. Saeki. 1995. Mechanisms of ice gouging. Proc. 5th International Offshore and Polar Engineering Conference, The Hague, The Netherlands, **2**, 398-402.

Kioka, S., Y. Yasunaga, U. Watanabe and H. Saeki. 2000. Evaluation of ice forces acting on seabed due to ice scouring. Proc. 10th International Offshore and Polar Engineering Conference, Seattle, USA, **1**, 749-755.

Nogueira, A.C. and M. Paulin. 1999. Limit state design for northstar offshore pipeline. Offshore, **59**, **9**, 146-150.

Palmer, A.C., I. Konuk, J. Love, K. Been and G. Comfort. 1989. Ice scour mechanisms. Proc. 10th International Conference on Port and Ocean Engineering under Arctic Conditions, Lulea, Sweden, **1**, 123-132.

Wright, B., J. Hnatiuk and A. Kovacs. 1981. Multi-year pressure ridges in the canadian beaufort sea. Coastal Engineering, **5**, 125-145.

Yang, T.S. 1999. Ice Ridge Scour Model for Estimation of Arctic Pipeline Trench Depth. Master thesis, Korea Maritime University.

Yoon, KY., K. Choi and H.I. Park. 1997. A numerical simulation to determine ice scour and pipeline burial depth. Proc. 7th International Offshore and Polar Engineering Conference, Honolulu, USA, **2**, 212-219.